NBSIR 83-2761

# Development of Power System Measurements -- Quarterly Report January 1, 1983 to March 31, 1983

U.S. DEPARTMENT OF COMMERCE
National Bureau of Standards
Center for Electronics and Electrical Engineering
Electrosystems Division
Washington, DC 20234

October 1983

Prepared for:
Department of Energy
on of Electric Energy Systems
Independence Avenue, SW
ington, DC 20585

NBSIR 83-2761

# DEVELOPMENT OF POWER SYSTEM MEASUREMENTS -- QUARTERLY REPORT JANUARY 1, 1983 TO MARCH 31, 1983

R. E. Hebner, Editor

U.S. DEPARTMENT OF COMMERCE
National Bureau of Standards
Center for Electronics and Electrical Engineering
Electrosystems Division
Washington, DC 20234

October 1983

Prepared for:
Department of Energy
Division of Electric Energy Systems
1000 Independence Avenue, SW
Washington, DC 20585


U.S. DEPARTMENT OF COMMERCE, Malcolm Baldrige, *Secretary*
NATIONAL BUREAU OF STANDARDS, Ernest Ambler, *Director*

## Foreword

This report is intended to summarize the progress of five technical investigations during the second quarter of FY 1983. Although reasonable efforts have been made to ensure the reliability of the data presented, it must be emphasized that this is an interim report so that further experimentation and analysis may be performed before the conclusions from any of these investigations are formally published. It is therefore possible that some of the observations presented in this report will be modified, expanded or clarified by our subsequent research.

TABLE OF CONTENTS

LIST OF FIGURES

LIST OF TABLES

# DEVELOPMENT OF POWER SYSTEM MEASUREMENTS -- QUARTERLY REPORT
January 1, 1983 to March 31, 1983

R. E. Hebner, Editor

This report documents the progress on five technical investigations sponsored by the Department of Energy and performed by or under a grant from the Electrosystems Division, the National Bureau of Standards. The work described covers the period January 1, 1983 to March 31, 1983. This report emphasizes the errors associated with measurements of electric and magnetic fields, the characteristics of corona in compressed $SF_6$ gas, and the measurement of the space charge density in transformer oil, the development of active insulators, and interfacial phenomena.

Key words: electric fields; gaseous insulation; interfaces; liquid insulation; magnetic fields; partial discharges; $SF_6$; solid insulation; transformer oil.

## 1. INTRODUCTION

Under an interagency agreement between the U. S. Department of Energy and the National Bureau of Standards, the Electrosystems Division, NBS, has been providing technical support for DOE's research on electric energy systems. This support has concentrated on the measurement of electric and magnetic fields, the measurement of interfacial phenomena, and of partial discharge phenomena. The technical progress made during the quarter January 1, 1983 to March 31, 1983 is summarized in this report.

## 2. ELECTRIC AND MAGNETIC FIELD MEASUREMENTS
Subtask Nos: 01 and 02

The objectives of this investigation are to develop methods to evaluate and calibrate instruments which are used, or are being developed, to measure the electric field, conductivity, the space charge density, and current density in the vicinity of high-voltage transmission lines and in apparatus designed to simulate the transmission line environment and to provide electrical measurement support to other investigators' efforts to determine the effects of fields on biological systems.

During the current reporting period, the development of a standard ion source for experimentally calibrating aspiration-type ion counters has been considered theoretically. Operators of aspirator-type ion counters normally use the relationship

$$\rho = I/\Phi \quad , \tag{1}$$

where $\rho$ is the ion density, I is the measured ion current, and $\Phi$ is the air flow, to determine the ion density for air ions with mobilities greater than a certain critical value. Experimental attempts to check the validity of this relation have involved the use of ion sources with coaxial cylinder geometries [1]. Ions which are produced by corona on a center wire conductor

are measured with an ion counter mounted to the side of the cylindrical outer conductor. By measuring the electric field E, and current density J, at the surface of the outer cylinder, and assuming a value for the ion mobility K, the charge density is calculated from the relation

$$\rho = J/KE \qquad (2)$$

and compared with the result obtained with eq (1). With this approach the assumption is made that the electric field across the opening, created in the side of the cylinder for the ion counter, is unchanged by removal of the conducting surface. The validity of this assumption is examined theoretically for a parallel plate ion source geometry with obvious implications for the coaxial cylinder case. The parallel plate geometry is considered as part of an effort to evaluate the feasibility of using the NBS parallel plate apparatus as a standard ion source for calibration purposes.

The geometry for the problem is shown with a sketch in figure 1. A circular aperture is created in the top plate of an infinite parallel plate system; the diameter of the aperture is made equal to half the parallel plate spacing. The top plate is grounded and a voltage is applied to the bottom plate to produce an electric field between the plates. Cylindrical symmetry about the y-axis is assumed. The field calculation is performed without considering the presence of space charge and thus provides only a qualitative view of the field conditions between the plates. The influence of conductors normally in the ion counter as well as fringing fields from the ion counter are also not considered.

Using a finite element code, resident on NBS computers, field strength values at representative points between the plates were calculated. Plotted in figure 1 are values of the vertical field strength as a function of distance above the bottom plate (y) and the parameter x (fig. 1). For this model calculation it can be seen that perturbations of over 40% occur across the entrance to the ion counter. At a point midway between the parallel plates, a distance equal to the diameter of the aperture, the perturbation is as large as about 2%. While the above results are obtained with a number of simplifying assumptions, they do raise questions regarding the validity of the previously described procedure for experimentally checking the performance of ion counters using eq (2).

A second question associated with the use of eq (2) which merits attention is how the air flow, due to the operation of the aspiration-type ion counter, influences the movement of air ions as they traverse the distance between the parallel plates or the interelectrode region for the coaxial cylinder case. Use of eq (2) assumes that the ions move with a drift velocity $v_d$, given by the product of ion mobility and electric field strength KE. However, because of the air flow through the ion counter, the velocity of the ion near the entrance of the ion counter may be as large as the sum of the drift velocity and air velocity. An approximate view of the situation under non-turbulant flow conditions is shown in figure 2. The sampling of streamlines in figure 2 represents the solution to the two-dimensional orifice problem using a conformal mapping technique [2]. The velocities shown along the streamlines at representative points are relative to the uniform flow velocity (taken to be unity) well below the plane of the orifice. While only a two-dimensional treatment of the problem, the calculated contraction of the jet, after passing through the orifice, agrees closely with the experimental value obtained with

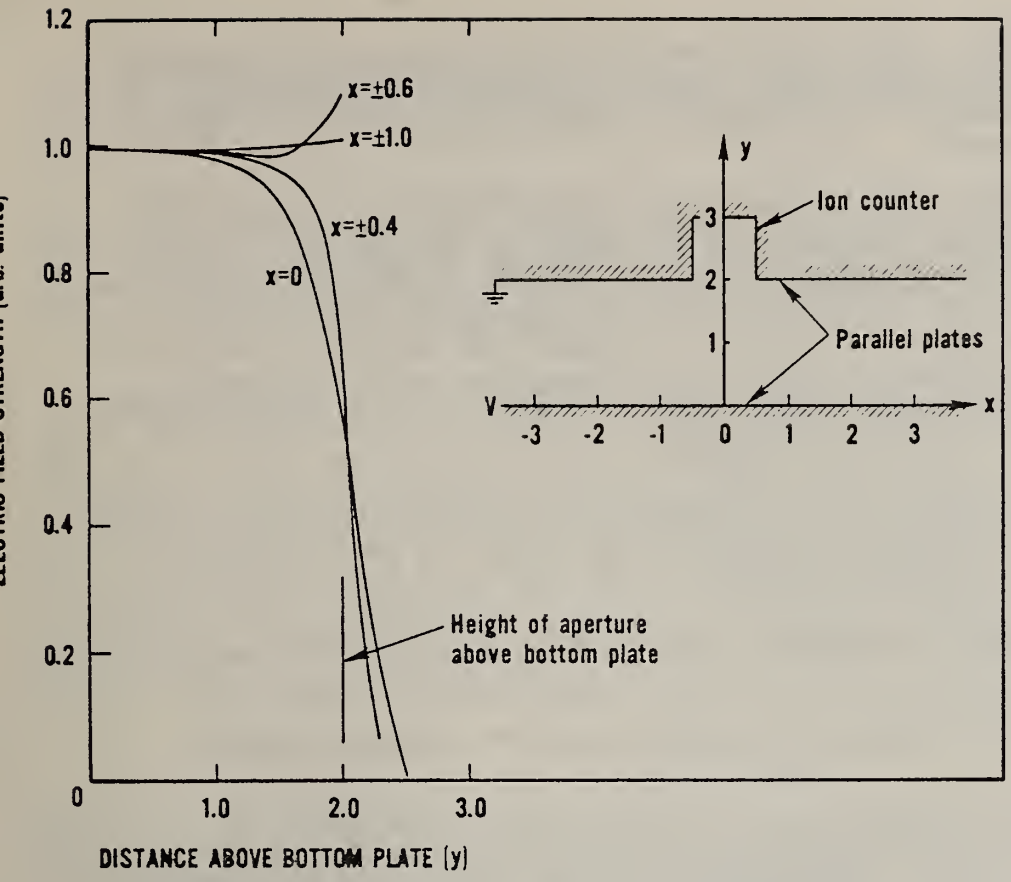


Figure 1. Variation of vertical electric field strength between parallel plates with ion counter connected to one plate. The diameter of the ion counter aperture is taken to be half the parallel plate spacing. Perturbations in the plane of the aperture are in excess of 40 percent.

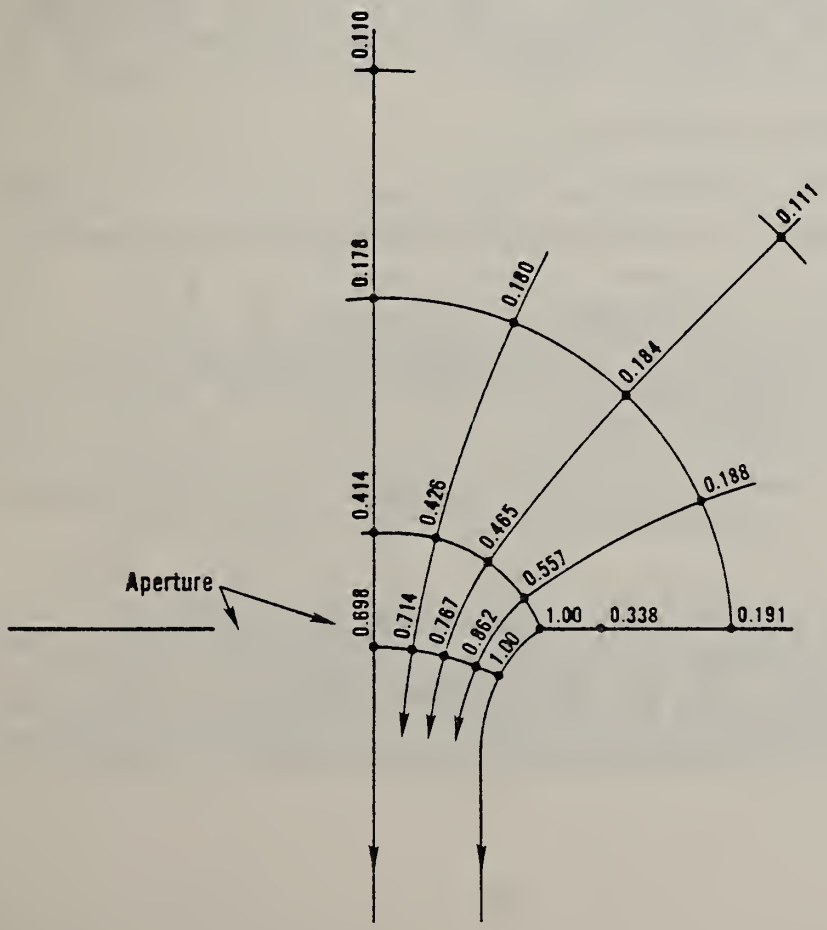


Figure 2. Flow pattern for two-dimensional orifice in flat plate. Relative velocities are indicated at representative points along the streamlines.

three-dimensional models. Other approximations to the actual problem include the assumption of a non-viscous fluid, neglecting the effects of the wall of the ion counter connected to the underside of the plate, and obstructions to the flow in the ion counter.

To place the results of the calculation into perspective, it should be noted that the air speed at the entrance of commercial ion counters can be as high as 1 m/s, which is comparable to drift velocities of positive air ions (about 1.4 m/s) in a field of about 10 kV/m [3]. Therefore, while only an approximation, the information in figure 2 suggests that the drift velocity of ions approaching an ion counter operating in a ground plane of a parallel plate system can be significantly perturbed while still at a distance comparable to the dimension of the ion counter opening.

The effects of an aperture on the electric field strength and air flow on the drift velocity of the ions near the entrance to an ion counter will be examined further during the next quarter.

For further information contact Dr. M. Misakian, (301) 921-3121.

## 3. TECHNICAL ASSISTANCE FOR FUTURE INSULATION SYSTEMS RESEARCH
Subtask No: 03

The objective of this project is to develop diagnostic techniques to monitor, identify, and predict degradation in future compressed gas electrical insulating systems under normal operating conditions. The focus is on the fundamental information and data needed to improve test design and performance evaluation criteria. The investigation of partial discharges (corona) in gaseous dielectrics is emphasized. This phenomenon gives rise to degradation of the gas under high electrical stress which leads to breakdown. Measurement of partial discharge inception in highly nonuniform fields may prove to be a preferred method to determine dielectric strength of electronegative gases.

The planned activities for FY83 include:

1) Preparation of conference and archival papers on the effect of radiation in enhancing electric discharge initiation near a positively stressed electrode in compressed $SF_6$ and $O_2$;

2) Extension of our previous measurements of the production rates of oxyfluorides in $SF_6$ corona discharges to include negative discharges as well as other gas pressures and discharge power levels, and preparation of the results for publication in an archival paper;

3) Identification of the predominant gaseous decomposition products from corona in one or more of the following gas mixtures: $SF_6 + N_2$, $SF_6 + CO_2$, and $SF_6 + c\text{-}C_4F_8 + CHF_3$;

4) Evaluation of a thin-film, aluminum oxide hygrometer probe for calibration of a gas chromatograph-mass spectrometer (GC/MS) used to measure trace quantities of water vapor in $SF_6$ and other gaseous dielectrics, and extension of our previous measurements on the effects of trace levels of $H_2O$ on electron avalanche growth and corona discharge characteristics in $SF_6$;

5) Design and construction of a drift tube-mass spectrometer system to evaluate measurements proposed to identify and characterize corona-generated ion species in air, $SF_6$, and other gas dielectrics.

Activity 1 has been completed, and during the past quarter a paper describing the results of our measurements and theoretical analysis was accepted for publication in the Journal of Applied Physics. Most of the work conducted during the past reporting period was related to activity 2, and the results of this work are highlighted below.

Measurements of the production rates of the oxyfluorides $SOF_2$, $SO_2F_2$, and $SOF_4$ in $SF_6$ point-plane corona discharges have been extended to negative polarities as well as to other gas pressures and discharge power levels. Results which have been analyzed to date for $SOF_2$ and $SO_2F_2$ are summarized in tables 1 and 2, respectively. Indicated in these tables are the polarities of the discharge (the polarity of the voltage applied to the more highly stressed electrode), the gas pressures, the average discharge power, and the corresponding production rates expressed in nanomoles per joule at the indicated accumulated energies U dissipated in the discharge. The rates given are extracted from fits to data from gas analysis using a gas chromatograph-mass spectrometer (GC/MS) which were of the form

$$C = B + AU^{1+\varepsilon} , \tag{3}$$

where C is the oxyfluoride concentration in moles and A, B, and $\varepsilon$ are fitting parameters which are assumed to be constant for each set of discharge conditions. The production rates are found from the expression

$$dC/dU = A(1 + \varepsilon)U^{\varepsilon} . \tag{4}$$

The concentrations C are calculated from the calibrated GC/MS single ion responses using the method given in our previous quarterly report. In the cases where more than one ion was used to determine the concentration for a given species, the results for the different ions were averaged. For example, some of the results in table 1 for $SOF_2$ represent averages of data from ions with mass-to-charge ratios of 86 and 67 corresponding respectively to the predominant ion species $SOF_2^+$ and $SOF^+$ observed in the mass spectra.

The results given in the tables exhibit the trends described in our previous report; namely, for positive corona the production rates for both $SOF_2$ and $SO_2F_2$ at a given gas pressure tend to decrease with increasing discharge power, and at the lowest pressure (116 kPa) there is an enhancement in the production of $SO_2F_2$ relative to $SOF_2$. In addition, results obtained during the past quarter, as shown in the tables, indicate a significant polarity effect. Not only are the production rates for both species seen to drop in going from positive to negative polarity, but also the ratio of $SOF_2$ to $SO_2F_2$ production increases by more than a factor of two.

In view of the fact that these data must still be regarded as preliminary, it would be premature at this stage to speculate on the causes of the polarity effect. There is reason to believe, however, that a large change in production rates resulting from switching of polarities may be an indication of the relative importance of ion-molecule reactions in the formation of the final neutral decomposition species. It is clear that more data are needed on the pressure and power dependence of oxyfluoride production from negative corona in $SF_6$.

Table 1. Measured production rates for $SOF_2$ in $SF_6$ at the different indicated gas pressures, discharge powers, and polarities.

| Polarity | Gas pressure (kPa) | Ave. power (mW) | Measured production rates (n·mol/J) (U = 5 kJ) | (U = 10 kJ) | (U = 15 kJ) |
|---|---|---|---|---|---|
| Positive | 116 | 804 | 0.24 | 0.37 | 0.48 |
| | 200 | 54 | 3.39 | 4.54 | -- |
| | 200 | 335 | 2.83 | 3.95 | 4.78 |
| | 200 | 777 | 1.60 | 2.52 | 3.31 |
| | 300 | 198 | 1.71 | 2.98 | 4.12 |
| | 300 | 430 | 1.29 | 1.95 | 3.49 |
| | 300 | 945 | 0.75 | 1.13 | 1.44 |
| Negative | 200 | 230 | 0.76 | 0.93 | 1.05 |
| | 200 | 586 | 0.55 | 0.63 | 0.68 |

Table 2. Measured production rates for $SO_2F_2$ in $SF_6$ at the different indicated gas pressures, discharge powers, and polarities.

| Polarity | Gas pressure (kPa) | Ave. Power (mW) | Measured production rates (n·mol/J) (U = 5 kJ) | (U = 10 kJ) | (U = 15 kJ) |
|---|---|---|---|---|---|
| Positive | 116 | 804 | 0.30 | 0.49 | 0.65 |
| | 200 | 54 | 3.09 | 4.25 | -- |
| | 200 | 154 | 2.84 | 4.15 | -- |
| | 200 | 335 | 2.25 | 2.93 | 3.43 |
| | 200 | 777 | 1.23 | 1.67 | 2.00 |
| | 300 | 198 | 1.14 | 1.68 | 2.10 |
| | 300 | 430 | 1.33 | 1.59 | 1.76 |
| | 300 | 945 | 0.57 | 0.80 | 0.97 |
| Negative | 200 | 230 | 0.11 | 0.22 | 0.35 |
| | 200 | 586 | 0.26 | 0.30 | 0.33 |

Further tests were carried out during this quarter to determine the major sources of error associated with these measurements. Sources that have been identified and considered include: 1) fluctuations and drift in discharge power (this is more a problem with positive than with negative corona, and most significant at higher power levels); 2) fluctuations in chromatograph background levels; 3) drift and nonlinearities in GC/MS response; and 4) errors associated with volume and gas pressure determinations and surface absorption during calibration sample preparations. Of these, at present the drift in GC/MS response appears for most experiments to be the largest source of uncertainty. The uncertainty due to this effect is estimated to be less than ±25% of the rates given in the tables. Although some further adjustments in the rates may be necessary, we believe that the numbers given in this report are correct to within an overall uncertainty of ±35%.

During the next quarter, we plan to continue the measurements of oxyfluoride production rates from corona in $SF_6$ as described in this report. In particular, more measurements will be carried out for negative corona discharges at different gas pressures and discharge power levels. Some measurements for positive polarity will be repeated to assess reproducibility, and to verify our estimates of uncertainties. Further consideration will be given to the possible sources of error in the measurement of production rates, and a search will be made for a set of GC/MS operating conditions which will minimize uncertainties due to oscillations of the background level in the chromatograph output which has become a problem for measurements performed at certain gas pressures. An attempt will be made to calibrate the response of the GC/MS to trace water vapor content in $SF_6$ using a thin-film aluminum oxide hygrometer probe.

For further information contact Dr. R. J. Van Brunt, (301) 921-3121.

## 4. OPTICAL MEASUREMENTS FOR INTERFACIAL CONDUCTION AND BREAKDOWN IN INSULATING SYSTEMS
Subtask No: 04

The objectives of this investigation are to develop apparatus and appropriate procedures for the optical measurements of interfacial electric field and space-charge density in materials for electric power equipment and systems, to understand the interfacial prebreakdown and breakdown processes in specific insulating systems, and to demonstrate the applicability of the developed instrumentation and the procedures in the development and design of future systems.

Last quarter a method was developed to perform field measurements in transformer oil which rendered low voltage, steady-state fields electro-optically visible. The method consisted of capacitively coupling an impulse to the electrode upon which a steady-state voltage was present. This method increased the observable Kerr effect by several orders of magnitude. The cell was installed with a polytetrafluoroethylene (PTFE) interface. In this arrangement, it was not possible to observe any field distortions near the interface even when water was added to the system and the temperature was increased to 120°C. To explain these observations it was hypothesized that the space charge displayed an onset which could not be reached before the interface would break down. The present quarter's activities examined this question further but the primary accomplishment has been further measurements of the Kerr coefficient as a function of temperature and light wavelength.

During the present quarter we were able to provide preliminary measurements of the electro-optical Kerr coefficient for the visible spectrum at room temperature (24°C) and at 97°C. A xenon flashtube light source was used with a monochrometer to provide the wavelength-selected light with an approximate uncertainty of ±15 nm. In order to provide simultaneous measurements of both the unpolarized light intensity and the light transmitted through the cell because of the Kerr effect, half of the image of the electrodes was covered by a neutral density filter, and the other half was covered by the analyzing polarizer (see fig. 3).

This method of observing both the incident light intensity and the Kerr effect at the same time is necessary whenever the light source does not produce the same intensity from shot to shot (as in the case of our xenon source). Under these circumstances, the detector was operated in the two-track scan mode to obtain profiles of the light between the plates in both regions of interest -- in the regions of the neutral density filter and of the analyzing polarizer (see fig. 3).

It is sufficient to note that data taken in this way provide two intensity measurements: I is the intensity due to the Kerr effect, and $I_m$ is the incident light intensity. The Kerr effect is then expressed by

$$I/I_m = \sin^2((\pi/2)(V/V_m)^2), \tag{5}$$

where the lowest voltage necessary to produce maximum transmitted intensity is $V_m$ which is related to the Kerr coefficient B and the cell parameters, i.e., the plate spacing d, and the plate length l, by

$$B = d^2/(2lV_m^2) . \tag{6}$$

The cell constant is obtained from eq (5)

$$V_m = V[(2/\pi)\sin^{-1}((I/I_m)^{1/2})]^{-1/2}, \tag{7}$$

where V is the applied voltage.

The Kerr coefficient as a function of wavelength for two temperatures is shown in figure 4. The detector system made a 1 μs recording at the peak of a 120 kV pulse. The data show a decrease in the Kerr coefficient for higher temperatures which is largest in the orange area of the visible spectrum. The variation of the Kerr effect with wavelength is larger -- changing about 30% over the visible spectrum -- for room temperature oil, than at the higher temperature.

The precision of these data is around ±10%, however, the accuracy is less certain, probably ±25%. the reason for the lack of accuracy is most likely the documented optical activity of the tank windows. This manifests itself in a voltage dependent Kerr coefficient (see fig. 4). Optical activity of windows would affect the lower voltage data more than at higher voltages. We chose to operate at 120 kV peak which would occasionally break down the gap.

Further cautions in handling this type of a system come from the monochrometer A grating will cause a small amount of scattering of light at wavelengths other

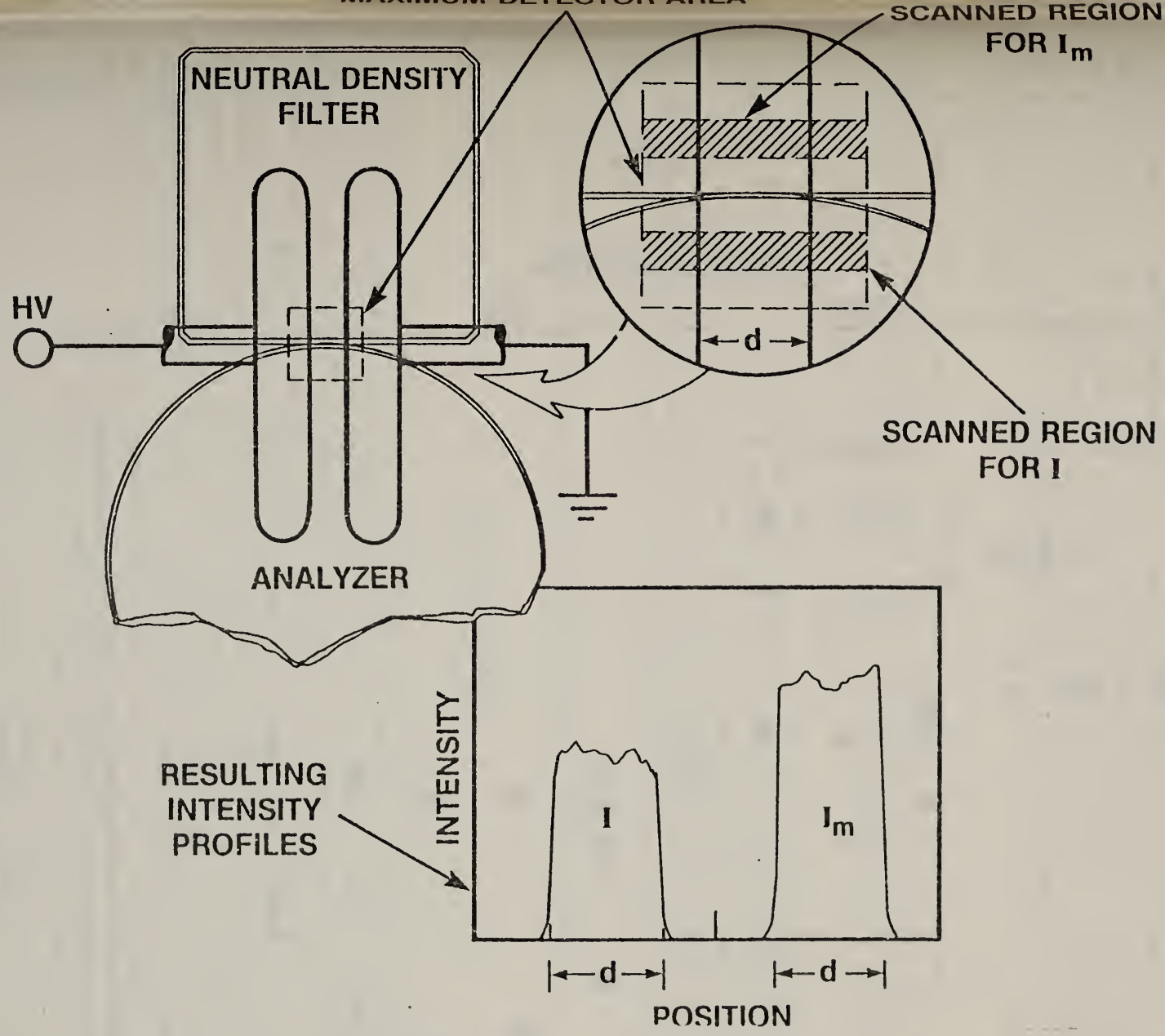


Figure 3. View of electrode system looking into the light beam from the position of the detector. The upper half of the area between the plates is covered by a neutral density filter to reduce the amount of light to avoid overloading the detector. The lower half of the area between the plates is covered with the analyzing polarizer to exhibit the Kerr effect. This method of making Kerr-effect measurements provides a means to measure the incoming light intensity at the same time the Kerr effect is observed, eliminating possible errors due to light source intensity changes from shot to shot. The wide, thin rectangles show the regions which were scanned by the detector.

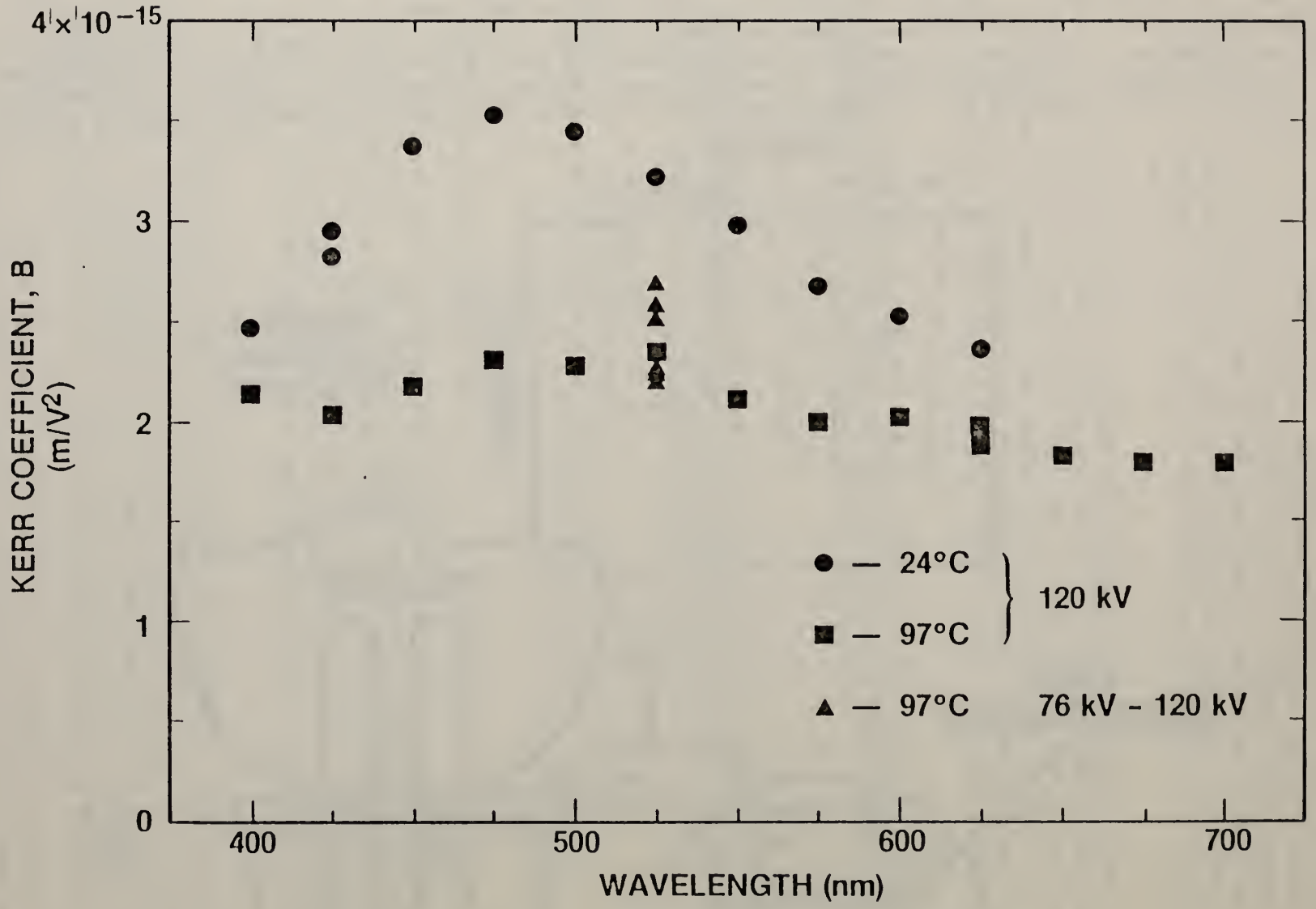


Figure 4. Kerr coefficient of transformer oil for the visible spectrum at 24°C and 97°C. These data were all taken at the peak of a 120 kV pulse. The precision of these data are indicated by the two points at 425 nm for room temperature oil and at 625 nm for the 97°C oil. The solid data points are all taken at the same voltage. The points marked "▲" are taken over a range of pulse voltage -- from 72 kV to 120 kV peak.

than what is selected. This scattered light becomes important at the ends of the visible spectrum where either the detector is less sensitive, the liquid becomes more absorbing, or the light source lacks intensity. For this reason, the data reported here are most reliable in the region 650 nm to 450 nm.

These results demonstrate that a measurement system can be made and calibrated to provide measurements of the Kerr coefficient as a function of temperature and wavelength. Although the present system suffers from an absolute calibration due to unaccounted optical activity of the windows, these data show that there are no fundamental obstacles which would prevent the construction of a system capable of accurate measurements should there be a need for such accuracy in the future. It is sufficient here to note the trends and identify possible problems.

Attempts will be made during the upcoming quarter to complete the measurements to determine space charge onset phenomena for steady-state voltages. Some progress was made this quarter, but additional measurements are required. It is anticipated that this question, along with the question about the water content affecting space charge, will be answered.

The cell-tank system for the examination of the effects of temperature upon the strength of a paper interface parallel to the field will be designed and built next quarter. This system will permit the rapid replacement or removal of the interfacial material after each breakdown, thus, the effects due to opening the system to replace the interface will be minimized. The system will permit an accurate comparison of the electrical strength with and without the interface present.

For further information contact Dr. E. F. Kelley, (301) 921-3121.

## 5. ACTIVE INSULATORS
Subtask No: 04

As a continuing effort to study the effects of active insulator assembly on power transmission lines under lightning, the mathematical model developed in the previous quarter was implemented to consider cases in which lightning strikes a transmission line conductor directly. As a worst case scenario, the operating voltage was assumed to have the same polarity as the lightning strike and have its maximum peak voltage; this would introduce the maximum stress on the insulator assembly. The lightning current was rated at 50 kA and struck at the middle of the transmission line. Results indicated that the maximum current passing through an active insulator assembly decreased linearly as the tower resistance increased (see fig. 5). Regardless of tower resistance, the maximum current passing through the substation arrester was 1.2 kA. On the other hand, without active insulators, the maximum current was found to be 38 kA. Even though active insulator assemblies could reduce the duty of station arresters significantly, the large current passing through these insulators poses a serious threat to the integrity of the insulator assembly itself. Appropriate measures to protect the insulators are essential, such as ground wires which should be provided to protect the transmission line from direct hits.

The second phase of this project is to develop a model for a three-phase system. The effects on adjacent phases can also be investigated. The basic

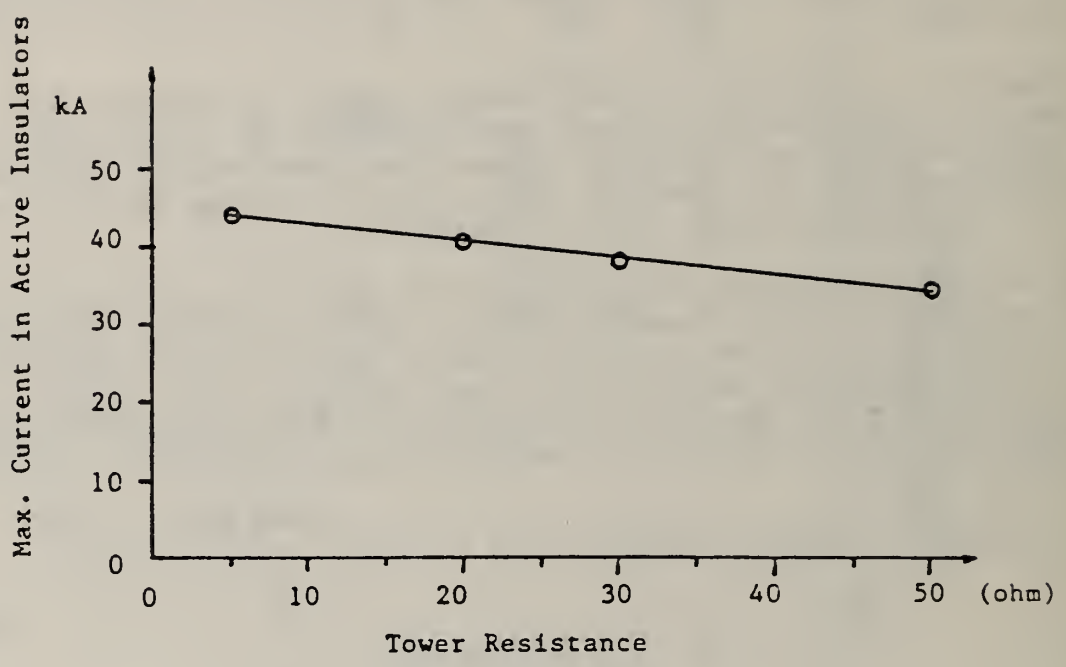


Figure 5. Maximum current passing through active insulators decreases as tower resistance increases.

model is similar to the single-phase model: instead of single values, the parameters are expressed as vectors and matrices. The Bergeron model for the three-phase system can first be expressed in the modal domain. Using phase-modal transformation, the nodal voltage is evaluated in the phase domain. The general transformation of all parameters and variables is expressed as:

$$[Z']_{\phi}^{-1} = [T][Z']_{m}^{-1}[T]^{-1} \tag{8}$$

$$[F]_{\phi} = [T][F]_{m}[T]^{-1} \tag{9}$$

$$[I'_{n,n-1}(t-\tau)]_{\phi} = [T][I'_{n,n-1}(t-\tau)]_{m} \tag{10}$$

$$[i_{n-1,n}(t-\tau)]_{\phi} = [T][i_{n-1,n}(t-\tau)]_{m} \tag{11}$$

$$[U_{n}(t-\tau)]^{\phi} = [T][U_{n}(t-\tau)]_{m} \ . \tag{12}$$

In all parameters and variables, the modal domain values are expressed as sequence values.

The propagation time $\tau$ is a vector, since the propagation time for each sequence is different as line parameter sequence varies. For the calculation of node voltage with active insulator assembly, the resultant voltage equation is

$$[(KU_{n}(t))^{\alpha}]_{\phi} + 2[Z']_{\phi}^{-1}[U_{n}(t)]_{\phi} + [I'_{n,n-1}(t-\tau)]_{\phi} + [I'_{n,n+1}(t-\tau)]_{\phi} = 0 \ . \tag{13}$$

Using Newton's iteration method the approximated solution for eq (13) can be obtained. A simplified flow chart for implementing this model is shown in figure 6.

For further information contact Dr. T. C. Cheng, (213) 743-6938.

## 6. INVESTIGATION OF INSULATOR SURFACE FLASHOVER IN GAS
Subtask No: 04

The objective of this investigation is to determine and describe the basic processes leading to the flashover of insulator surfaces in vacuum and pressurized gas. Specific objectives include: (1) measurement of insulator surface currents to determine the role of geometry and material parameters on the surface currents and the role of surface currents in insulator surface charging and flashover; (2) electro-optical measurement of insulator/gas and insulator/vacuum interfacial electrical fields prior to flashover; and (3) development of analog and numerical techniques to predict interfacial electric fields for applicable geometries and established surface charge distributions.

Surface currents have been measured this quarter in vacuum and nitrogen, along polymethylmethacrylate, PMMA, insulators. Results are similar to those reported last quarter. Additional measurements have, however, been obtained this quarter for additional pressures and electrode separations. Additionally, analyses have been performed to improve the understanding of the observed current behavior.

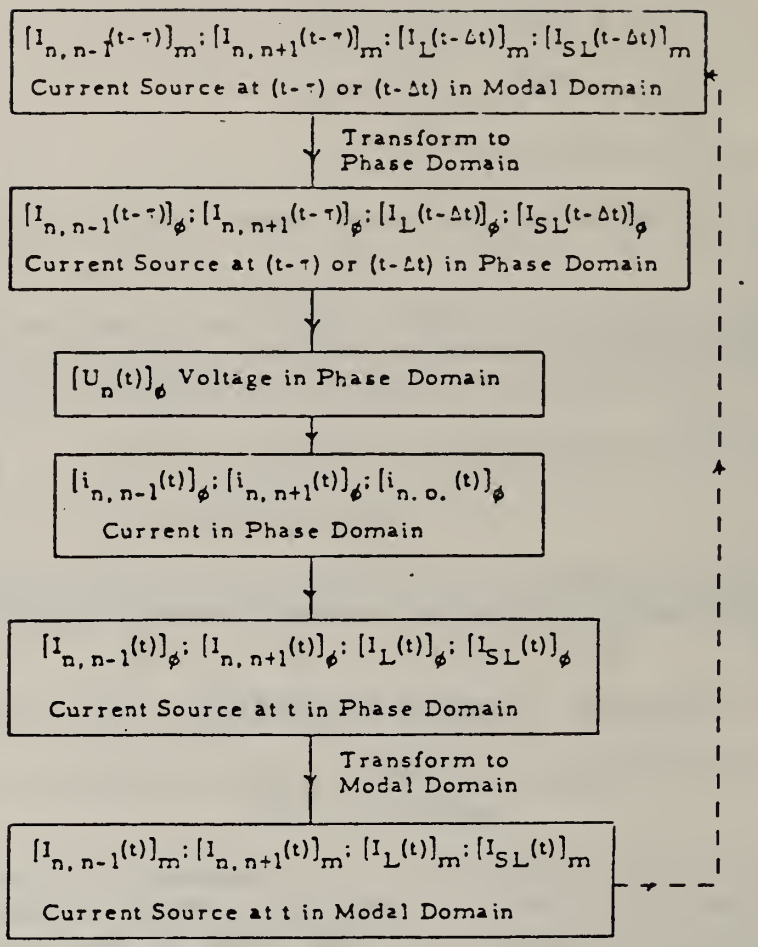


Figure 6. Flow chart for implementing three-phase model.

Surface currents have been measured in vacuum and nitrogen. The observed surface current behavior in vacuum differs from the behavior in gas. It has been previously reported, and also observed this quarter, that surface currents in vacuum, along 60 Hz excited PMMA insulators, have three components: (1) a low amplitude, randomly occurring component. This component is observed at relatively low voltages and occurs in the form of short duration pulses, near the excitation peak; (2) a longer duration component. This component begins to occur at higher voltages (above a threshold). The peak of this component occurs, in time, before the voltage peak and, in many cases, extinguishes before the voltage peak; and (3) a third component arises at higher voltages. This component is large in amplitude and is approximately in phase with the excitation.

Based upon this observed behavior, it is being postulated that: component (1) is due to partial discharges across the gap, either away from or on the insulator surface; component (2) is due only to current along the insulator and is the current responsible for charging the insulator; and component (3) is due to field emission current flowing from the cathode to the anode, away from the insulator surface.

Analyses have been performed this quarter to relate the observed surface behavior to the postulated mechanisms. It has been determined that the time integral of current component (2) yields a value of charge equal to $1 \times 10^{-5}$ C/m$^2$. This value is comparable to charge values previously measured using the electro-optical field measurement technique. This implies that current component (2) is associated with insulator surface charging. Analyses have also been performed on the component (3) current data. The observed current/voltage relationship of this component has been determined and compared to the relationship predicted for field emission by the Fowler-Nordheim equation. Agreement is good for the limited data analyzed. These preliminary analysis results imply that component (3) current is therefore due to current flowing between the cathode and the anode with negligible interaction with the insulator surface.

Additional PMMA/nitrogen interfacial current measurements have been made this quarter. The observed surface current behavior in gas is different than that observed in vacuum. The results show that the current flows in short pulses occurring during the excitation. Relatively long duration (type (2)) current components have not been observed. The observed emission has a definite voltage threshold. This threshold voltage is very close to the voltage necessary for insulator surface flashover in nitrogen.

The observed temporal shape of these short duration surface current pulses, observed in vacuum and gas, is indicative of the impulses' response of the measurement system and is therefore not significant. However, the response amplitude and repetition period are significant and indicative of preflashover (possibly surface charging) event size and period of occurrence.

A multi-channel analyzer (MCA) has therefore recently been obtained to enable computer data acquisition and analysis regarding the pulse amplitude, frequency, and number. Time has been spent this quarter designing pulse shaping and computer interfacing circuitry. The system is essentially complete and consists of a pulse shaper, a computer, and graphics output. The system is now operational but has not been used to acquire or process surface data. Completion of a necessary computer link should permit use of this system next quarter. The objective of the planned measurements is to quantify the relationships

between size and frequency of surface current pulses and various insulator characteristics (such as geometry and material) in both vacuum and gas.

The surface fields, associated with the measured surface currents, have been previously electro-optically measured and reported. This quarter modifications to the experimental arrangement have continued to reduce charge injection into the electro-optical sensing liquid and resulting charging of the liquid for 60 Hz excitation. It is anticipated that these modifications will be complete and initial measurements made by the first of May.

The measurement techniques described above measure surface currents and electric fields associated with insulator surface charging. It is postulated that this surface charging reduces the insulator hold-off strength due to local electric field enhancement established by the surface charge. Analog and digital analysis techniques have been developed to predict the insulator fields associated with the surface charge.

An electrolytic tank has been constructed to predict surface fields associated with various surface charge distributions likely to occur. The tank construction has been completed and consists of a large PMMA container, a step motor driven probe, and a computer data acquisition and manipulation system. The entire system is capable of determining the electric field components associated with various insulator shapes and permittivities. The results are produced in the form of three dimensional plots of electric field E, as a function of position along and away from a dielectric interface. Results have been obtained for insulator cone frustums having angles $\theta$ of 30°, 45°, and 60° ($\theta$ is the angle between the insulator and electrode surface) and for relative permittivities $\varepsilon_r$, of 3, 9, and 35. Results are shown in figures 7 and 8 and are indicative of other results also obtained for geometrical and permittivity changes. The electrode and interface locations are indicated in figure 7(a). The results show the spatial variation of the electric field and the value of the maximum field $E_{MAX}$. The results show that $E_{MAX}$ increases for increases in both $\theta$ and $\varepsilon_r$. It has also been determined that, with this geometry, the field at one electrode is decreased, while the field at the other electrode is increased. This analysis technique is presently being used to determine the effect of uncharged insulator shape and permittivity on triple junction fields. Triple junction fields play an important role in insulator charging processes.

A computer based, finite difference, numerical technique has also been developed to determine the surface fields associated with various geometries and surface charge. Typical results are shown in figure 9 for $\theta = 45°$ and $\varepsilon_r = 9$. These results compare favorably with those obtained using the electrolytic tank. These results are also being used to determine the effect of various geometries and surface charge on the inter-electrode fields.

In summary, surface current measurements have been made in vacuum and nitrogen using the previously reported electrical diagnostic system. For vacuum, the results have been analyzed and related to previously, electro-optically, measured surface charge values and voltage/current performance predicted from field emission equations. The results imply that surface charging and gap field emission are both occurring, but have different 60 Hz voltage thresholds. Gas data presently imply that surface currents are of short duration and sporatic. A computer-aided data acquisition and analysis system is being implemented to permit more systematic analysis of the data. Analog and numerical

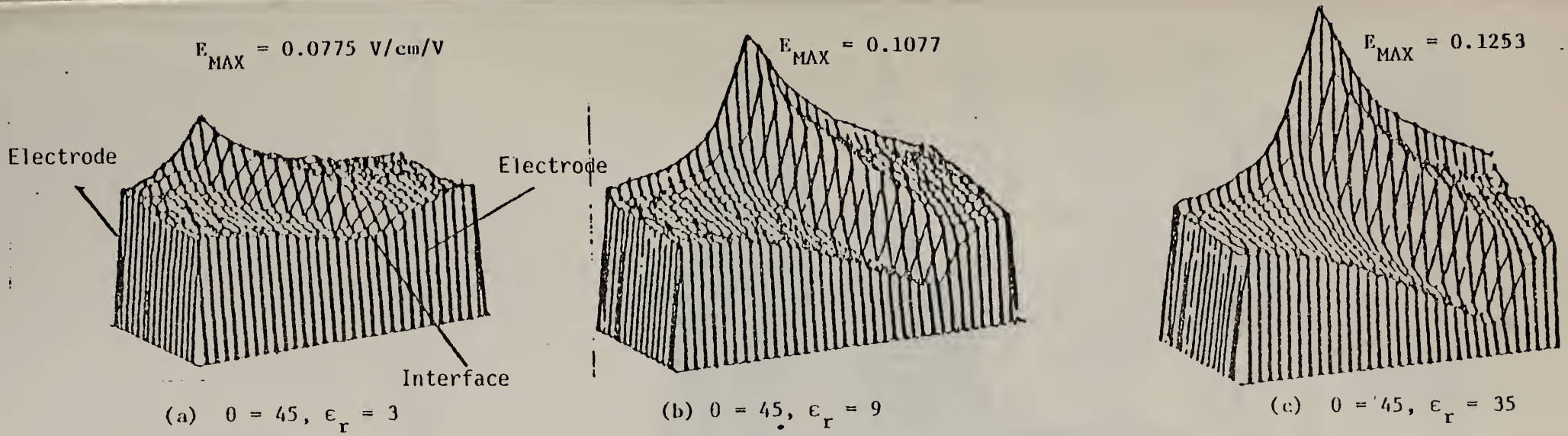


Figure 7. Plots showing the E field distribution for different dielectric mismatches.



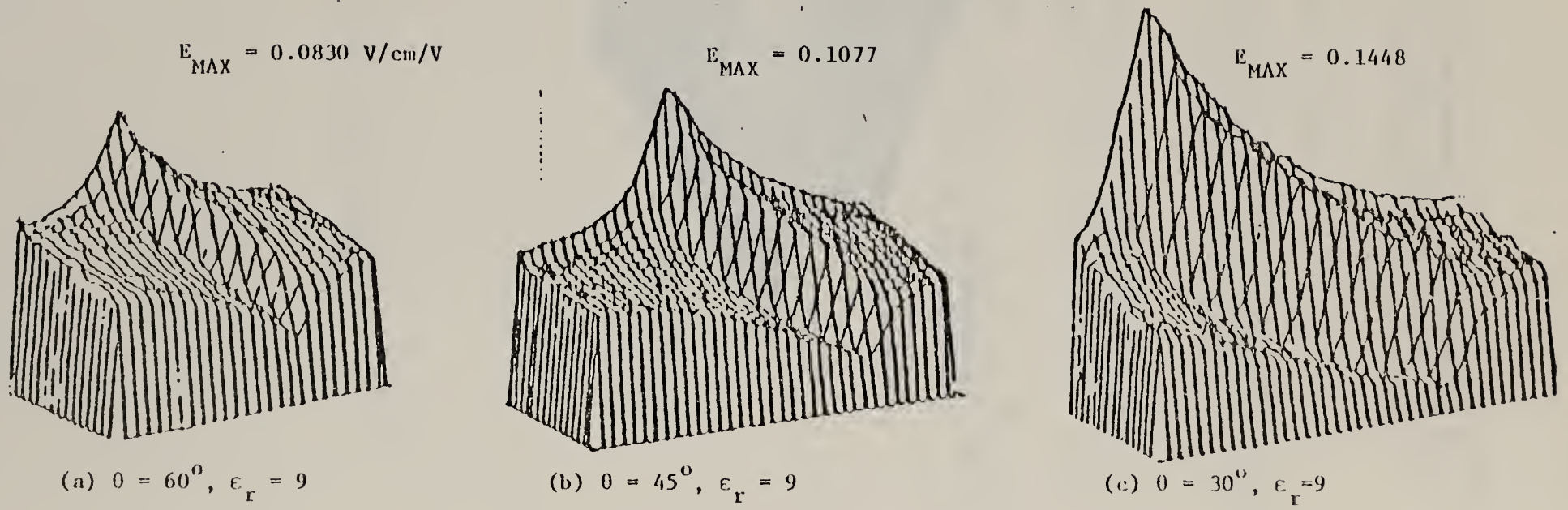


Figure 8. Plots showing the E field distribution for different insulator angles.

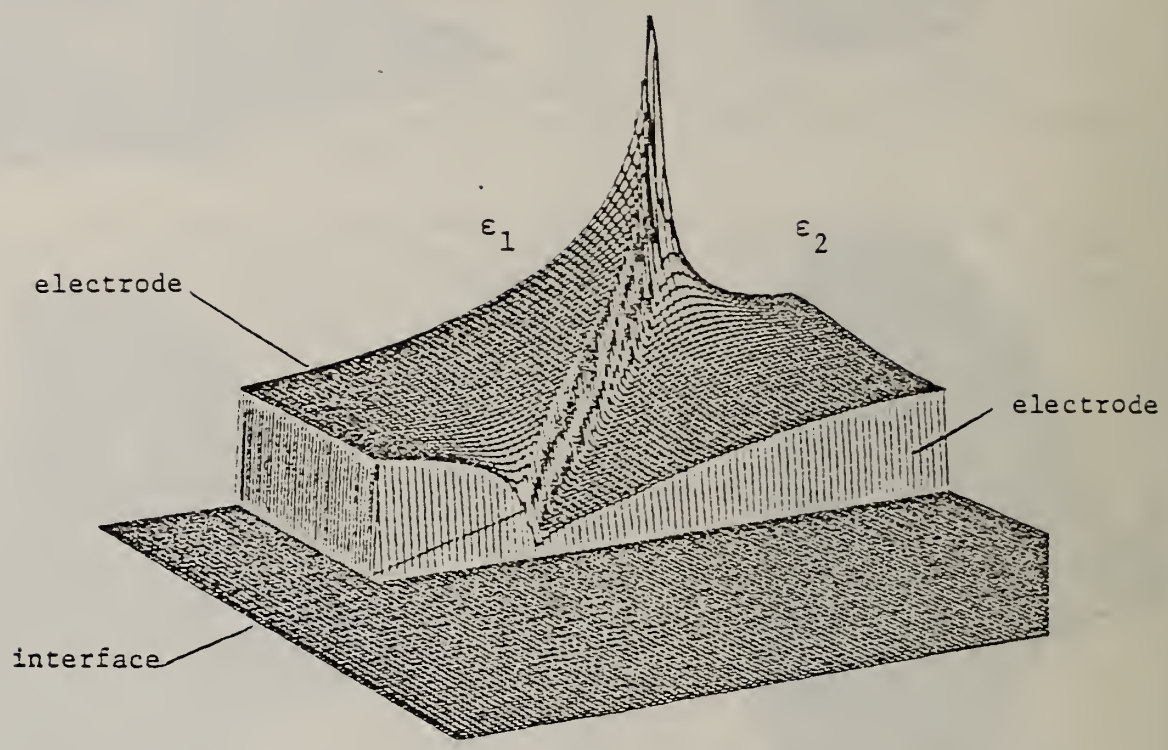


Figure 9. Electric field distribution between electrodes with permittivity interface ($\varepsilon_2/\varepsilon_1 = 9$), $E_{MAX}$ = 3.76 V/cm/volt applied.

techniques have been developed and have been used to calculate electric fields associated with various insulator material and geometry. These results are being used to predict the role of insulator shape, permittivity, and surface charge on breakdown, and to assist in the understanding of the experimental surface charge and field data obtained.

Tasks to be accomplished next quarter include:

1) The MCA will be used to acquire and process surface current measurements in vacuum and nitrogen. The current behavior, as a function of voltage, insulator material, and insulator geometry, will be determined. Measurements will also be done in $SF_6$.

2) The electro-optical diagnostic system will be completed and preliminary glass/gas interfacial measurements made. It is anticipated that no charge injection will occur into the sensing liquid. Field nonuniformities will then be due only to surface charge and geometry effects.

3) Numerical and analog analyses will continue to relate surface fields to surface charge. The capability is being developed to determine what surface charge is associated with the electro-optically measured surface field.

For further information contact Dr. J. E. Thompson, (803) 777-7304.

## 7. REFERENCES

[1] T. D. Bracken and B. C. Furumasu, Field and Ion Current Measurements in Regions of High Charge Density Near Direct Current Transmission Lines, p. 544, Proceedings of the Conference on Cloud Physics and Atmospheric Electricity, (American Meterological Society, Boston, 1978). For a description of related studies conducted at the National Bureau of Standards, see Report NBSIR 81-2267, 1980 Annual Report to the Department of Energy and Report NBSIR 82-2527, 1981 Annual Report to the Department of Energy.

[2] L. V. Bewley, Two-Dimensional Fields in Electrical Engineering, p. 146, (Dover, New York, 1963).

[3] M. Misakian, Generation and Measurement of DC Electric Fields with Space Charge, J. Appl. Phys., Vol. 52, pp. 3135-3144, 1981.

NBS-114A (REV. 2-8C)

| U.S. DEPT. OF COMM. BIBLIOGRAPHIC DATA SHEET (See instructions) | 1. PUBLICATION OR REPORT NO. NBSIR 83-2761 | 2. Performing Organ. Report No. | 3. Publication Date September 1983 |
|---|---|---|---|

4. TITLE AND SUBTITLE

Development of Power System Measurements -- Quarterly Report
January 1, 1983 to March 31, 1983

5. AUTHOR(S)

R. E. Hebner, Supervisory Physicist

6. PERFORMING ORGANIZATION (If joint or other than NBS, see instructions)

NATIONAL BUREAU OF STANDARDS
DEPARTMENT OF COMMERCE
WASHINGTON, D.C. 20234

7. Contract/Grant No.

8. Type of Report & Period Covered

9. SPONSORING ORGANIZATION NAME AND COMPLETE ADDRESS (Street, City, State, ZIP)

Prepared for
Department of Energy
Division of Electric Energy Systems
1000 Independence Avenue, S. W.
Washington, DC 20585

10. SUPPLEMENTARY NOTES

☐ Document describes a computer program; SF-185, FIPS Software Summary, is attached.

11. ABSTRACT (A 200-word or less factual summary of most significant information. If document includes a significant bibliography or literature survey, mention it here)

This report documents the progress on five technical investigations sponsored by the Department of Energy and performed by or under a grant from the Electrosystems Division, the National Bureau of Standards. The work described covers the period January 1, 1983 to March 31, 1983. This report emphasizes the errors associated with measurements of electric and magnetic fields, the characteristics of corona in compressed $SF_6$ gas, and the measurement of the space charge density in transformer oil, the development of active insulators, and interfacial phenomena.

12. KEY WORDS (Six to twelve entries; alphabetical order; capitalize only proper names; and separate key words by semicolons)

electric fields; gaseous insulation; interfaces; liquid insulation; magnetic fields; partial discharges; $SF_6$; solid insulation; transformer oil

13. AVAILABILITY

☒ Unlimited

☐ For Official Distribution. Do Not Release to NTIS

☐ Order From Superintendent of Documents, U.S. Government Printing Office, Washington, D.C. 20402.

☒ Order From National Technical Information Service (NTIS), Springfield, VA. 22161

14. NO. OF PRINTED PAGES

15. Price $8.50